Numerical Simulation on the TIBL Structure in Shoreline Areas with a 2D Higher-Order Turbulence Closure Model

JIANG WEIMEI AND WU XIAOMING

Department of Atmospheric Sciences, Nanjing University, Nanjing City, China

ZHOU JINGNAN

Nanjing Institute of Meteorology, Nanjing City, China

(Manuscript received 15 February 1993, in final form 8 June 1994)

ABSTRACT

A 2D higher-order turbulence closure model for research on the structure of the thermal internal boundary layer (TIBL) has been developed in this paper. The mean quantities (temperature and wind), as well as their turbulent moments and their distribution under the TIBL, were computed. Results of numerical simulation show that under the initial condition of onshore flow and surface temperature on land being higher than on water, 1) the profile of the TIBL on shore can be identified by the distributions of the mean wind and temperature, and during the integration hours there is an unstable stratified region over land that extends upward and inland gradually; 2) the shape of the profiles of the TIBL is roughly in concordance with observed profiles, but there are some differences, obviously, between the results computed by the formula of $h \sim x^{1/2}$ and the results of the numerical experiment; and 3) $\overline{u'^2}$, $\overline{v'^2}$, $\overline{w'^2}$, and $\overline{u'w'}$, $\overline{\theta'w'}$ and their general features are well reproduced by the model. It is shown that the numerical model is feasible and effective.

1. Introduction

During the last two decades, several approaches have been taken to study the thermal internal boundary layer (TIBL) structure in shoreline areas. It is well known that simulated TIBL depends on turbulent models and that the turbulent mode will affect fine structure of the TIBL. The PBL higher-order turbulence closure model is most suitable to reveal the turbulence condition, because it may predict directly some characteristic atmospheric turbulence quantities and their distributions in detail. Such a simulation gives a far more faithful representation in far more detail than traditional eddy diffusivity approaches and may avoid the arbitrarity for determining the eddy diffusivity. The higher-order turbulence closure technique is based on the ensemble average statistics and is discussed by Reynolds (1970), Donaldson (1973), Mellor and Yamada (1974), and others. Deardorff (1972) used it first to simulate neutral and unstable PBL and showed that it is an attractive method for calculating the structure of the turbulent flow. Requirement of the computer time is relatively modest. Here we attempt to use the model developed in this paper to study the structure of the TIBL in a shoreline area and employ this approach as the first step toward the modeling of the fine structure of TIBL.

2. The model

a. The equations and mathematic formulation

The coordinates x, y, z denote rectangular axes toward the shoreline, along the shoreline, and upward in vertical direction, respectively, and the mean and fluctuating velocities are represented by u, v, w and u', v', w', respectively. It is assumed that a shoreline is straight and unlimited and that the flow is horizontally homogeneous along the shoreline and its properties depend only on x, z, and t. The hydrostatic assumption was made in the model for the mean flow. Considering a horizontally homogeneous and incompressible flow, a set of governing equations is as follows:

$$\frac{\partial u}{\partial t} + u\frac{\partial u}{\partial x} + w\frac{\partial u}{\partial z} = -\frac{1}{\rho}\frac{\partial P}{\partial x} + fv - \frac{\partial \overline{(u'w')}}{\partial z} \quad (1)$$

$$\frac{\partial v}{\partial t} + u\frac{\partial v}{\partial w} + w\frac{\partial v}{\partial z} = -\frac{1}{\rho}\frac{\partial P}{\partial y} - fu - \frac{\partial \overline{(v'w')}}{\partial z} \quad (2)$$

$$-\frac{1}{\rho}\frac{\partial P}{\partial z} = g \quad (3)$$

$$\frac{\partial \theta}{\partial t} + u\frac{\partial \theta}{\partial x} + w\frac{\partial \theta}{\partial z} = -\frac{\partial \overline{(\theta'w')}}{\partial z} \quad (4)$$

$$\frac{\partial u}{\partial x} + \frac{\partial w}{\partial z} = 0. \quad (5)$$

Corresponding author address: Prof. Jiang Weimei, Department of Atmospheric Sciences, Nanjing University, Nanjing 210008, China.

A set of equations on the second-order moments $\overline{\theta'w'}$, $\overline{u'w'}$, $\overline{v'w'}$, and so on have to be set up (see Haugen 1973). Using the closure scheme of Mellor and Yamada (1974), the pressure terms, the dissipation terms, and the diffusion terms in equations on the second-order moments may be given. It is assumed that the influence of the Coriolis force is smaller than the production term of the second-order moment, and it may be ignored in these equations. Then the equations of $d\overline{(u_i'u_j')}/dt$, $d\overline{(\theta'u_i')}/dt$, $d\overline{\theta'^2}/dt$, and dq^2/dt where $q = (\overline{u'^2} + \overline{v'^2} + \overline{w'^2})^{1/2}$ can be obtained in suitable form.

In the model a variable isentropic surface boundary was used (Pielke 1974) and the terrain-following coordinate system x^*, y^*, z^* was introduced (Pielke 1984). The final set of the second-order closure equations in new coordinate system is

$$\frac{du}{dt} = -\theta\frac{\partial\pi}{\partial x^*} - g\frac{z^*}{\bar{s}}\frac{\partial s}{\partial x^*} + fv - \frac{\bar{s}}{s}\frac{\partial(\overline{u'w'})}{\partial z^*} \tag{6}$$

$$\frac{dv}{dt} = -\theta\frac{\partial\pi}{\partial y^*} - fu - \frac{\bar{s}}{s}\frac{\partial(\overline{v'w'})}{\partial z^*} \tag{7}$$

$$\frac{d\theta}{dt} = -\frac{\bar{s}}{s}\frac{\partial(\overline{\theta'w'})}{\partial z^*} \tag{8}$$

$$\frac{\partial u}{\partial x^*} + \frac{\partial w^*}{\partial z^*} + \frac{1}{s}\left(\frac{\partial s}{\partial t} + u\frac{\partial s}{\partial x^*}\right) = 0 \tag{9}$$

$$\frac{\partial\pi}{\partial z^*} = -\frac{s}{\bar{s}}\frac{g}{\theta} \tag{10}$$

$$\frac{d(\overline{u'w'})}{dt} = -\frac{\bar{s}}{s}\overline{w'^2}\frac{\partial u}{\partial z^*} + \frac{g}{\theta_0}\overline{\theta'u'} - \frac{q}{3l_1}(\overline{u'w'}) + c_1\frac{\bar{s}}{s}q^2\frac{\partial u}{\partial z^*} + \left(\frac{\bar{s}}{s}\right)^2\frac{\partial}{\partial z^*}\left[2q\lambda_1\frac{\partial}{\partial z^*}(\overline{u'w'})\right] \tag{11}$$

$$\frac{d(\overline{u'w'})}{dt} = -\frac{\bar{s}}{s}\overline{w'^2}\frac{\partial v}{\partial z^*} + \frac{g}{\theta}\overline{\theta'v'} - \frac{q}{3l_1}(\overline{v'w'}) + c_1\frac{\bar{s}}{s}q^2\frac{\partial v}{\partial z^*} + \left(\frac{\bar{s}}{s}\right)^2\frac{\partial}{\partial z^*}\left[2q\lambda_1\frac{\partial}{\partial z^*}(\overline{v'w'})\right] \tag{12}$$

$$\frac{d(\overline{u'v'})}{dt} = -\frac{\bar{s}}{s}\overline{u'w'}\frac{\partial v}{\partial z^*} - \frac{\bar{s}}{s}\overline{v'w'}\frac{\partial u}{\partial z} - \frac{q}{3l_1}\overline{u'v'} + \left(\frac{\bar{s}}{s}\right)^2\frac{\partial}{\partial z^*}\left[q\lambda_1\frac{\partial(\overline{u'v'})}{\partial z}\right] \tag{13}$$

$$\frac{d\overline{u'^2}}{dt} = -2\left(\frac{\bar{s}}{s}\right)\overline{u'w'}\frac{\partial u}{\partial z^*} - \frac{q}{3l_1}\left(\overline{u'^2} - \frac{q^2}{3}\right) + \left(\frac{\bar{s}}{s}\right)^2\frac{\partial}{\partial z^*}\left(q\lambda_1\frac{\partial\overline{u'^2}}{\partial z}\right) - \frac{2q^3}{3\Lambda_1} \tag{14}$$

$$\frac{d\overline{w'^2}}{dt} = 2\frac{g}{\theta_0}\overline{\theta'w'} - \frac{q}{3l_1}\left(\overline{w'^2} - \frac{q^2}{3}\right) + 3\left(\frac{\bar{s}}{s}\right)^2\frac{\partial}{\partial z^*}\left(q\lambda_1\frac{\partial\overline{w'^2}}{\partial z}\right) - \frac{2q^3}{3\Lambda_1} \tag{15}$$

$$\frac{dq^2}{dt} = -2\overline{u'w'}\left(\frac{\bar{s}}{s}\right)\frac{\partial u}{\partial z^*} - 2\overline{v'w'}\left(\frac{\bar{s}}{s}\right)\frac{\partial v}{\partial z^*} + 2\frac{g}{\theta_0}\overline{\theta'w'} + \left(\frac{\bar{s}}{s}\right)^2\frac{\partial}{\partial z}\left[q\lambda_1\left(\frac{\partial q^2}{\partial z^*} + 2\frac{\partial\overline{w'^2}}{\partial z^*}\right)\right] - \frac{2q^3}{\Lambda_1} \tag{16}$$

$$\frac{d\overline{(\theta'w')}}{dt} = -\overline{w'^2}\left(\frac{\bar{s}}{s}\right)\frac{\partial\theta}{\partial z^*} - \overline{u'w'}\left(\frac{\partial\theta}{\partial x^*} - \frac{z^*}{s}\frac{\partial s}{\partial x}\frac{\partial\theta}{\partial z^*}\right) + \frac{g}{\theta_0}\overline{\theta'^2} + \frac{q}{3l_2}\overline{\theta'w'} + \left(\frac{\bar{s}}{s}\right)^2\frac{\partial}{\partial z^*}\left[2q\lambda_2\frac{\partial(\overline{\theta'w'})}{\partial z}\right] \tag{17}$$

$$\frac{d\overline{(\theta'u')}}{dt} = -\overline{\theta'w'}\left(\frac{\bar{s}}{s}\right)\frac{\partial u}{\partial z^*} - \overline{u'w'}\left(\frac{\bar{s}}{s}\right)\frac{\partial\theta}{\partial z^*} - \overline{u'^2}\left(\frac{\partial\theta}{\partial x^*} + \frac{z^*}{s}\frac{\partial s}{\partial x}\frac{\partial\theta}{\partial z^*}\right) - \frac{q}{3l_2}\overline{\theta'u'} + \left(\frac{\bar{s}}{s}\right)^2\frac{\partial}{\partial z^*}\left[q\lambda_2\frac{\partial}{\partial z^*}(\overline{\theta'u'})\right] \tag{18}$$

$$\frac{d\overline{(\theta'v')}}{dt} = -\overline{\theta'w'}\left(\frac{\bar{s}}{s}\right)\frac{\partial v}{\partial z^*} - \overline{v'w'}\left(\frac{\bar{s}}{s}\right)\frac{\partial\theta}{\partial z^*} - \overline{v'w'}\left(\frac{\partial\theta}{\partial x^*} + \frac{z^*}{s}\frac{\partial s}{\partial x}\frac{\partial\theta}{\partial z^*}\right) - \frac{q}{3l_2}\overline{\theta'v'} + \left(\frac{\bar{s}}{s}\right)^2\frac{\partial}{\partial z^*}\left[q\lambda_2\frac{\partial}{\partial z}(\overline{\theta'v'})\right] \tag{19}$$

$$\frac{d\overline{\theta'^2}}{dt} = -2\overline{\theta'w'}\left(\frac{\bar{s}}{s}\right)\frac{\partial\theta}{\partial z^*} - 2\overline{\theta'u'}\left(\frac{\partial\theta}{\partial x^*} - \frac{z^*}{s}\frac{\partial s}{\partial x}\frac{\partial\theta}{\partial z^*}\right) + \left(\frac{\bar{s}}{s}\right)^2\frac{\partial}{\partial z^*}\left(q\lambda_3\frac{\partial\overline{\theta'^2}}{\partial z^*}\right) - 2\frac{q}{\Lambda_2}\overline{\theta'^2}. \tag{20}$$

b. The boundary conditions

Using an isentropic surface as the upper boundary condition, $\theta|z^* = s$ = constant. All of the turbulence quantities, the second-order moments, and mean gradients were set to zero at the upper boundary due to lack of knowledge of these quantities in the boundary layer, and the geostrophic relation was satisfied. The lower boundary conditions were $u|_0 = v|_0 = w|_0 = 0$; $\theta|_0 = \theta_g(t, x)$, where $\theta_g(t, x)$ was given based on the practice situation.

It is assumed in the model that 1) influence of the horizontal advection of the second-order moments is much smaller than the influence of the production term; 2) in the surface layer the turbulence timescale is much smaller than the timescale of local variation; and 3) the diffusion terms of the second order are small, and a set of diagnostic equations can be obtained from Eqs. (11)–(20):

$$\overline{u'w'} = \frac{3l_1}{q}\left(-\overline{w'^2}\frac{\bar{s}}{s}\frac{\partial u}{\partial z^*} + \frac{g}{\theta_0}\overline{\theta'u'} + c_1 q\frac{\bar{s}}{s}\frac{\partial u}{\partial z^*}\right)$$

$$\overline{v'w'} = \frac{3l_1}{q}\left(-\overline{w'^2}\frac{\bar{s}}{s}\frac{\partial v}{\partial z^*} + \frac{g}{\theta_0}\overline{\theta'v'} + c_1 q\frac{\bar{s}}{s}\frac{\partial u}{\partial z^*}\right)$$

$$\overline{u'v'} = \frac{3l_1}{q}\left(-\overline{u'w'}\frac{\bar{s}}{s}\frac{\partial v}{\partial z^*} - \overline{v'w'}\frac{\bar{s}}{s}\frac{\partial u}{\partial z^*}\right)$$

$$\overline{u'^2} = \frac{q^2}{3} + \frac{3l_1}{q}\left(-2\overline{u'w'}\frac{\bar{s}}{s}\frac{\partial u}{\partial z^*} - 2\frac{q^3}{3\Lambda_1}\right)$$

$$\overline{w'^2} = \frac{q^2}{3} + \frac{3l_1}{q}\left(2\frac{g}{\theta_0}\overline{\theta'w'} - \frac{2q^3}{3\Lambda_1}\right)$$

$$q^2 = \frac{\Lambda_1}{2q}\left[-2\overline{u'w'}\left(\frac{\bar{s}}{s}\right)\frac{\partial u}{\partial z^*} - 2\overline{v'w'}\frac{\bar{s}}{s}\frac{\partial v}{\partial z^*} + 2\frac{g}{\theta_0}\overline{\theta'w'}\right]$$

$$\overline{\theta'w'} = \frac{3l_2}{q}\left(-\overline{w'^2}\frac{\bar{s}}{s}\frac{\partial \theta}{\partial z^*} - \overline{u'w'}\frac{\partial \theta}{\partial x^*} + \frac{g}{\theta_0}\overline{\theta'^2}\right)$$

$$\overline{\theta'u'} = \frac{3l_2}{q}\left(-\overline{\theta'w'}\frac{\bar{s}}{s}\frac{\partial u}{\partial z^*} - \overline{u'w'}\frac{\bar{s}}{s} - \overline{u'^2}\frac{\partial \theta}{\partial x^*}\right)$$

$$\overline{\theta'v'} = \frac{3l_1}{q}\left(-\overline{\theta'w'}\frac{\bar{s}}{s}\frac{\partial v}{\partial z^*} - \overline{v'w'}\frac{\bar{s}}{s}\frac{\partial \theta}{\partial z^*} - \overline{u'v'}\frac{\partial \theta}{\partial x^*}\right)$$

$$\overline{\theta'^2} = \frac{\Lambda_2}{2q}\left(-2\overline{\theta'w'}\frac{\bar{s}}{s}\frac{\partial \theta}{\partial z^*} - 2\overline{\theta'u'}\frac{\partial \theta}{\partial x^*}\right).$$

These equations were solved to obtained the second-order moment for the lower boundary conditions.

The lateral boundary conditions were divided into upstream and downstream boundaries: the former was a fixed inflow boundary condition, and the latter was the gradient outflow, that is, $\partial A/\partial x|_z = +L = 0$, where A represented the meteorological elements and L was the distance from shoreline.

c. Numerical aspects and computational conditions

In the model the horizontal grid interval was Δx = 2 km and the vertical grid had different intervals from the ground surface to the uppermost grid point. The number of grid points was 20 × 30. The time step Δt = 12 s was found to be stable.

The numerical integration in the model was performed by several different finite-difference schemes. In order to compute the first-order and second-order quantities, the leapfrog scheme was used. The scheme used for vertical advective terms was the central difference scheme. The scheme used for horizontal advective terms in the equations was the backward difference method. The scheme used for diffusion terms in the equations was the central difference in the middle point method. The time integrations for the terms of horizontal advection, vertical advection, vertical diffusion, pressure, and the dissipation were performed by the implicit difference scheme. The time integration for the other terms in the equations was performed fully by the explicit difference scheme.

3. Results

The mean fields of wind component, potential temperature, and the turbulence fields characterized by $\overline{u'^2}$, $\overline{w'^2}$, $\overline{u'w'}$, and $\overline{\theta'w'}$ and so on under the onshore flow and the TIBL condition were studied. In order to simulate the development of the TIBL, the upstream lateral boundary and initial field were such that there was an onshore flow condition and the surface temperature on land was higher than on water. The data report of the Nanticoke field study (Ministry of the Environment 1980) and the hourly vertical profiles of temperature and wind as a function of height obtained from minisonde flights at the MS1 site located in the shoreline area in that study were used. The day of 7 June 1979 was warm and mainly sunny with onshore winds from the south-southeast. Clouds developed in the afternoon.

The second-order moments of $\overline{u'^2}$, $\overline{v'^2}$, $\overline{w'^2}$ were set equal to 10^{-5} m s^{-2} and the other quantities were taken smaller than this value. The initialization for these quantities was performed by the 1D higher-order closure model. Meanwhile, these quantities may input into the 2D model as an initial field at the bottom boundary, but the temperature of the water surface was kept to be constant and the daily variation of the temperature of ground surface was given in form of a sine distribution: $\theta_1 = \theta_w + A\sin(2\pi t/T)$, where A was magnitude of the temperature variation and set to 20 K, θ_w was 298 K, and T was 86 400 s. Starting from 0800 EST, the numerical integration was performed up to 1700 EST.

a. Distributions of mean temperature and wind

The simulated mean fields of potential temperature θ during the integration hours were presented, for ex-

ample, in Fig. 1. Some features on distributions and its evolution simulated potential temperature fields under onshore flow condition may be revealed. The TIBL structure can be identified from these. There is an unstable stratification region over land and it extends up and toward inland gradually. It is obvious that the unstable region is a result of heating of the underlying surface on land and it is relative to the temperature difference between ground surface and water surface in shoreline area. So the TIBL height can be identified by the boundary of this unstable region.

The simulated field of the u component is presented in Fig. 2. In the TIBL it is relatively well mixed and its intensity increases gradually during the developing period of the TIBL inland. There are high and low regions of u separately in the PBL over shoreline area. Usually, the low-value region is over the high region and the intensity is in increasing tendency with time gradually until the increase in temperature stopped, and the intensity will decrease finally.

Comparisons between Figs. 1 and 2 show that the high region of u is basically in correspondence with unstable region, but the low-value region is usually over the unstable region. It is shown that in the TIBL, the intensity of onshore flow increases with the development of the TIBL. When they were separated from the

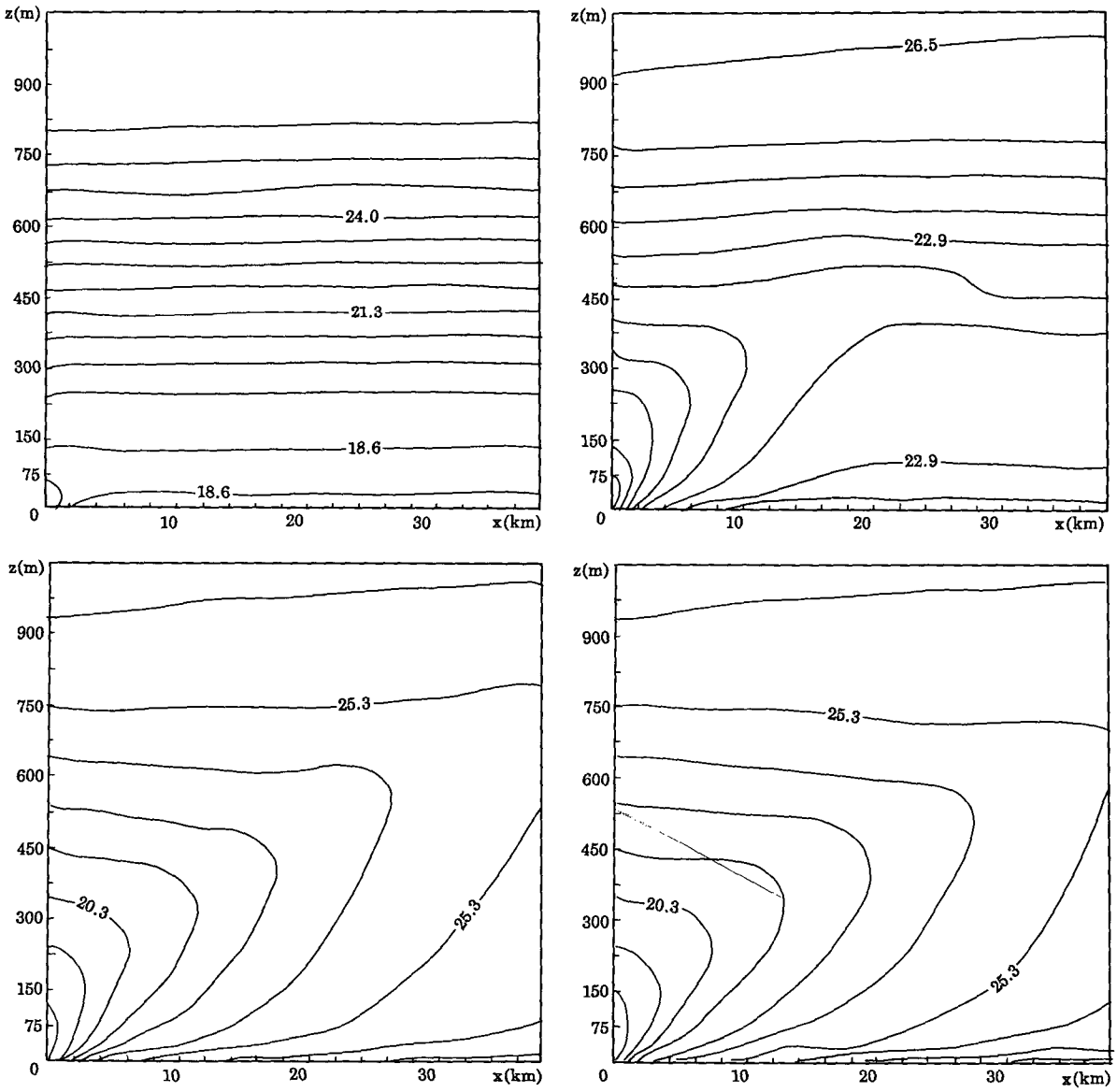

FIG. 1. Computed fields of mean potential temperature. (a) After integration time 1 h; (b) after integration time 3 h; (c) after integration time 5 h; (d) after integration time 7 h.

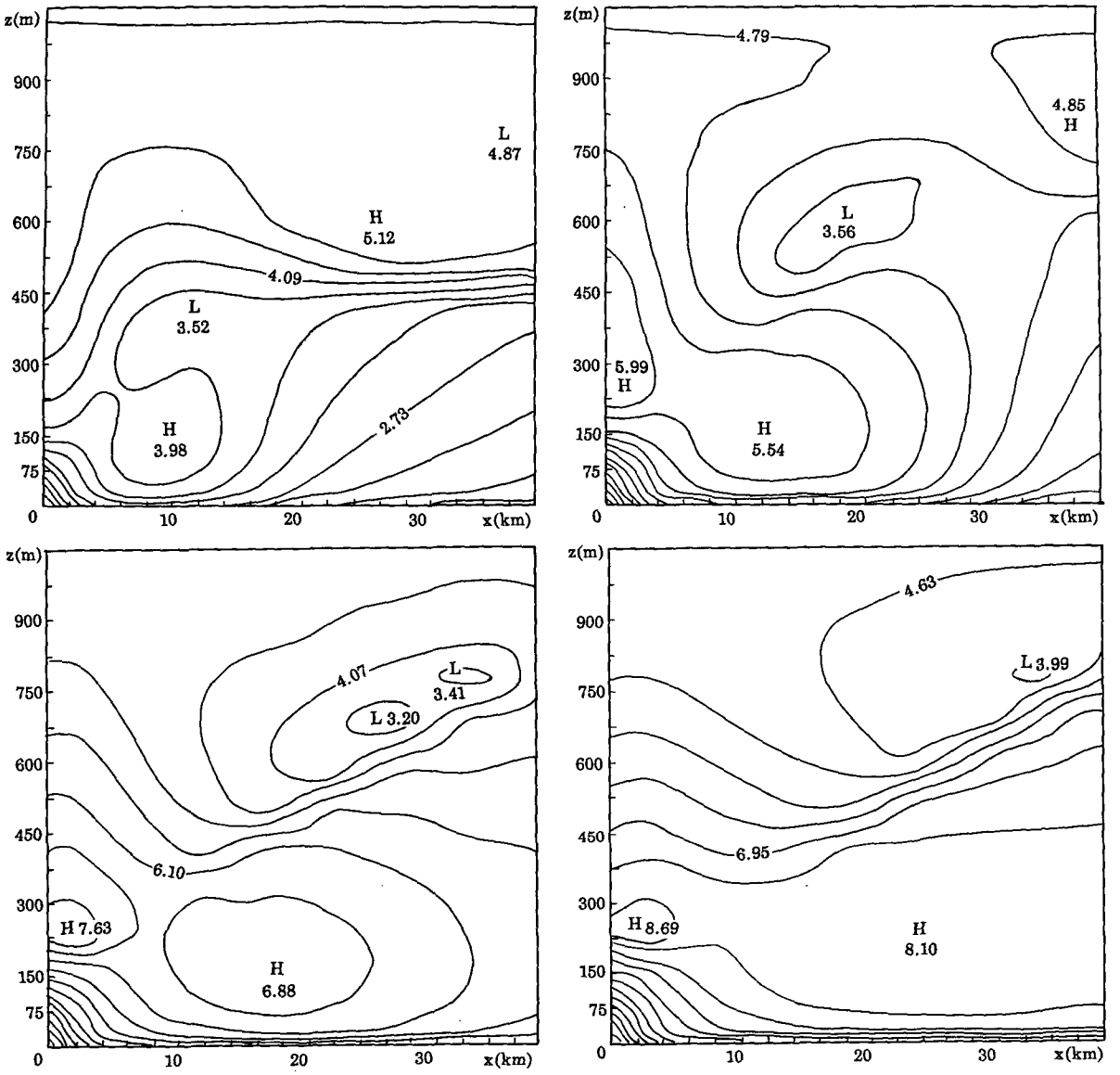

FIG. 2. Computed fields of mean horizontal wind component u (m s^{-1}). (a) After integration time 3 h; (b) after integration time 4 h; (c) after integration time 5 h; (d) after integration time 6 h.

prevailing wind, the high-value and low-value regions in Fig. 2 should be corresponded to onshore flow and offshore flow separately. If the prevailing wind is very weak, it would be expected that the local sea breeze will be more obviously developed. The model results of the vertical profiles of mean potential temperature and wind component u obtained from Figs. 1 and 2 are presented in Fig. 3. In Fig. 3 the variations of the TIBL height with the distance from shoreline can be determined usually according to the turning points on the wind profiles and temperature profiles.

b. The TIBL height

In general, there are two main factors, horizontal advection and vertical advection, for determining of the growth rate of the TIBL. It is believed that the TIBL height $h_i(x)$ is closely proportional to $x^{1/2}$ in field of air pollution meteorology (Ludwig 1985). In Fig. 4, however, there are obvious fluctuations and changing slope on the profiles, which is in accordance with the conclusion on observed profiles of Fritts et al. (1980). In Fig. 4 the maximum height of the TIBL is at the distances of 13 and 20 km from shoreline after integration of 2 and 3 h, respectively, and the growth rates of the TIBL height are also different from each other. Comparisons between model results and the wind field show that there is slightly increasing slope for the higher wind speeds, and the position of the maximum TIBL height is obviously related to the vertical advective transport by the wind. In Fig. 4 it cor-

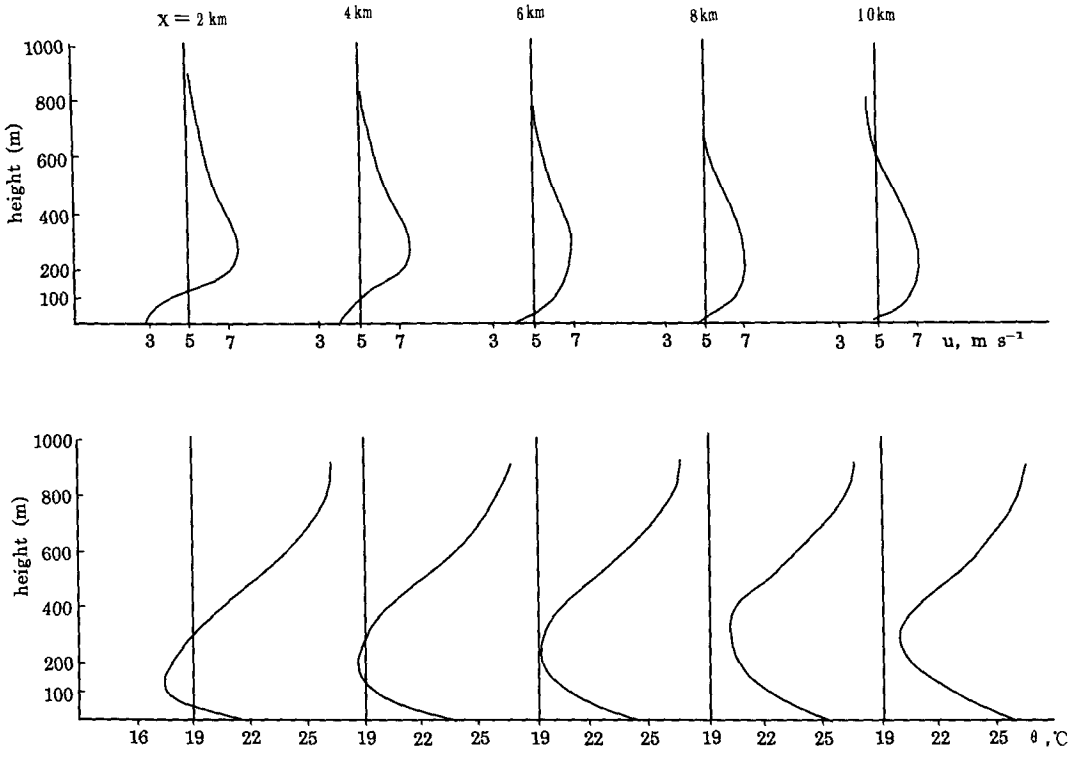

FIG. 3. Computed profiles of u and θ at different distances from the shoreline.
(a) Profiles of u (5 h) and of (b) θ (5 h).

responds with the convergence region of the onshore flow. It is believed that the nonmonotonous variations of the developing slope of the TIBL profiles with inland distance x are caused mainly by the mean wind field and vertical motion. It should also point out that the empirical models also have many limiting assumptions. Since such conditions rarely occur is the real world, the various formulations employed are thus limited—paving the way for more full-featured numerical models.

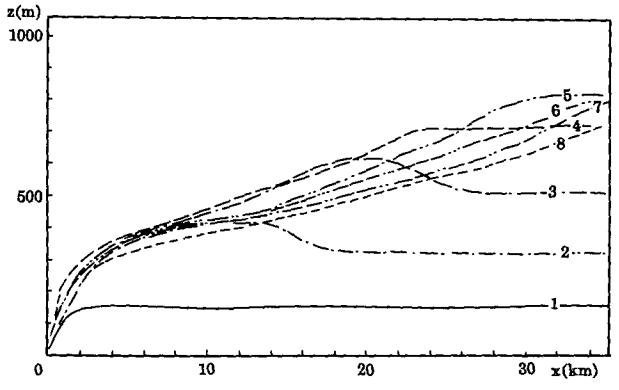

FIG. 4. Simulated TIBL profiles by numerical model in this paper at different integration time (hours: 1–8).

c. *Turbulence field*

1) THE VARIANCES OF VELOCITY COMPONENTS u', v', w'

The computed fields of $\overline{u'^2}$, $\overline{v'^2}$, and $\overline{w'^2}$ may be obtained, and, for example, the computed field of $\overline{w'^2}$ is presented in Fig. 5. The highest values of the variances are usually at low altitudes, where additional turbulence is caused by surface friction and there is strong thermal convection there due to heating of the ground surface. In the TIBL the turbulence intensity increases gradually from the shoreline upward and inland. The vertical profiles of $\overline{u'^2}$, $\overline{v'^2}$, $\overline{w'^2}$ at several inland distances from the computed fields may be obtained. It can be seen that one at the lower altitude usually is accompanied with a maximum center of $\overline{w'^2}$ and another in higher layer is relative to the position of the maximum region of velocity component u. It is considered that the former is governed by thermal factor and the latter is governed by the vertical shear of velocity component u. In other words, the turbulence energy is mainly produced by buoyancy (i.e., thermal mechanism), but the mechanical production in the TIBL is also noticeable. The turbulent structure from computed fields of the variances are in good qualitative agreement with observed fields.

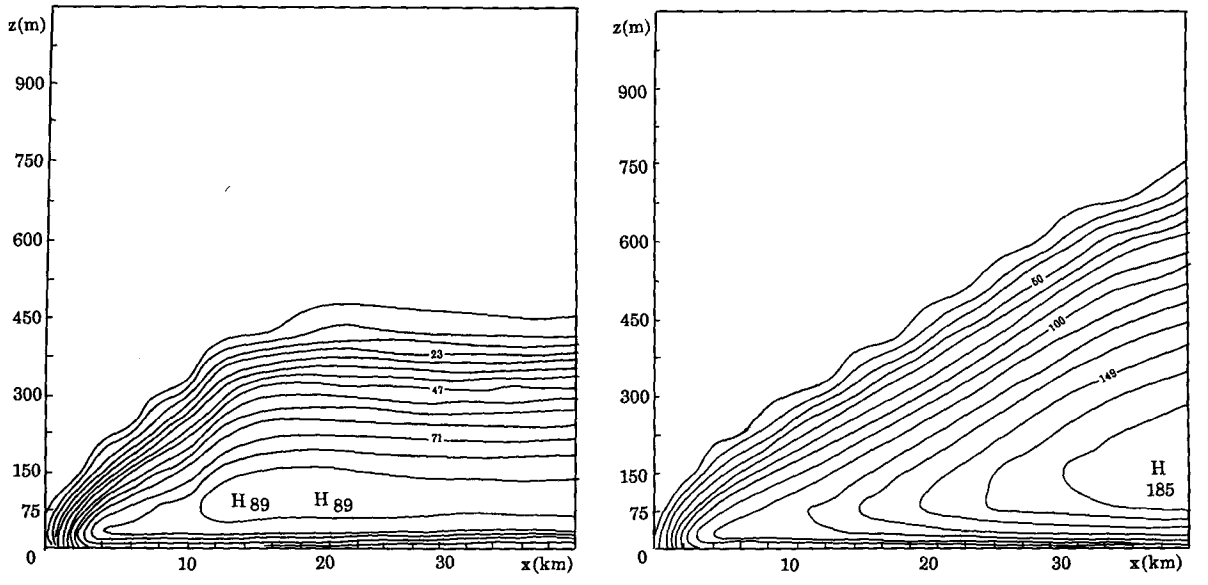

FIG. 5. Computed field of $\overline{w'^2}$, in (a) 3 h and (b) 5 h.

2) THE TURBULENCE FLUXES

The computed fields of the turbulent fluxes $\overline{u'w'}$ and $\overline{w'\theta'}$ are given in Figs. 6 and 7. Figure 6 shows downward transport of $\overline{u'w'}$ at low altitude and there is upward transport at the top of the TIBL, which is relative to the role of the entrainment and pressure gradient. The turning level from negative (downward) into positive (upward) is different at various integration times. In model results, $\overline{u'w'}$ is negative near ground surface and positive at levels of 70–300 m. In Fig. 7 there is large upward transport of $\overline{w'\theta'}$ near ground surface due to superadiabatic condition, and there is downward transport at the top of the TIBL. For example, at a site 4 km from shoreline, the $\overline{w'\theta'}$ is positive from ground surface layer to 150–200 m, but it decreases with increase in height. The top of the TIBL is roughly at this level in this case. This range of the positions of maximum values of $\overline{w'\theta'}$ increases gradually with increase in distance from shoreline. This is consistent with the general character of the convective boundary layer (Caughey and Palmer 1979).

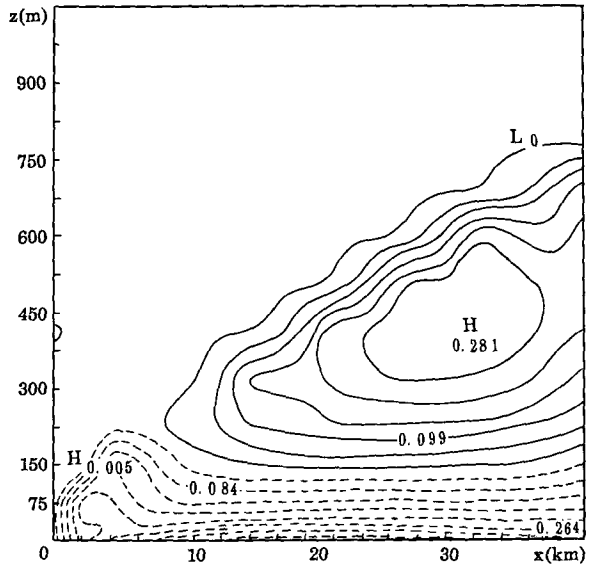

FIG. 6. Computed field of $\overline{u'w'}$, in 5-h case.

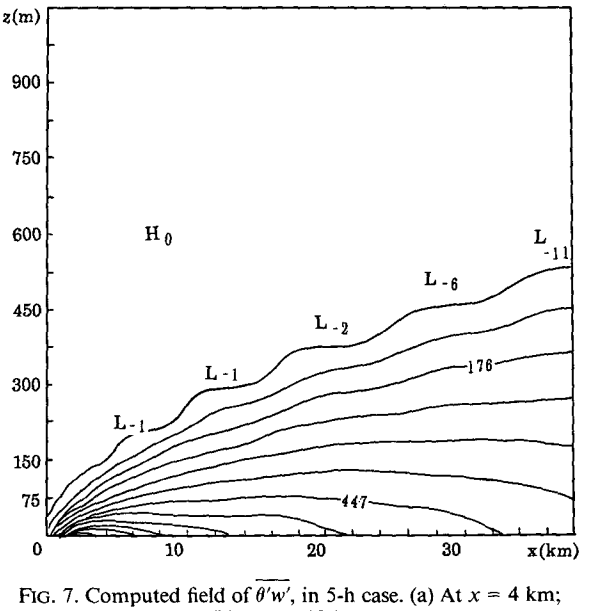

FIG. 7. Computed field of $\overline{\theta'w'}$, in 5-h case. (a) At x = 4 km; (b) at x = 10 km.

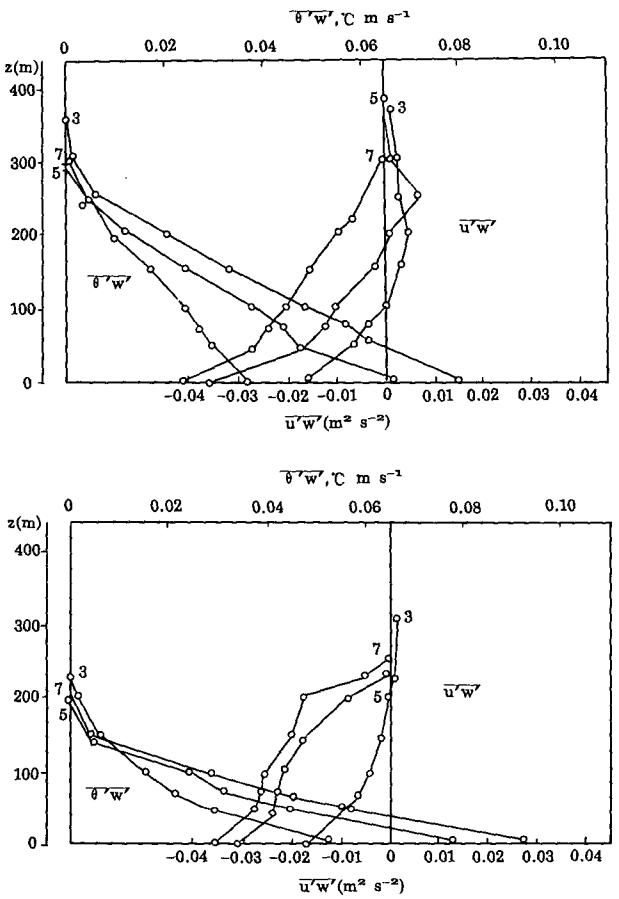

FIG. 8. Simulated profiles of the turbulent heat flux and momentum flux (in 3-, 5-, and 7-h cases).

In summary, a rapid decrease in the turbulence level is displayed obviously in the first few hundred meters. So the turbulence heat flux $\overline{w'\theta'}$ and momentum flux $\overline{u'w'}$ decreases quickly up to about 400–500 m and then slowly above. The behavior is quite similar to the dissipation rate of TKE, which presents a slight minimum at 400 m and shows a deficit in production of TKE (see Durand et al. 1989). The model results of $\overline{w'u'}$ and $\overline{w'\theta'}$ profiles, for example, at a 4-km site, are presented in Figs. 8a and 8b. It is similar to the results of $\overline{w'\theta'}$ and $\overline{w'u'}$ profiles observed by the Nanticoke II shoreline diffusion experiment (Ogawa et al. 1986).

4. Conclusions

The structure of the TIBL over a water–land transition area with onshore flow has been studied with a higher-order turbulence closure model (a 2D version). Because of the satisfactory and reproduction of mean and turbulence fields under the TIBL condition, the model can be used to reveal fine structure of the TIBL in the shoreline area. This is very interesting because measurements of the turbulence fields are very difficult to obtain. This is a preliminary effort and it is encouraging.

All of these show that the higher-order turbulence closure model is surely one kind of effective and potential tool for the study of the problems on the TIBL. Because it is cheaper than the large-eddy simulation models, it may obtain some fine descriptions of the turbulent flow in more detail, and it is better than the models used for the TIBL is some time away, our results suggest that it is well worth pursuing. It is certainly an improvement over the empirical model often used in air pollution modeling. But it also should be noted that a fully 3D prognostic model with some treatments of the ground–air exchanges would be necessary to simulate the TIBL in a coastal area and it would be more effective and useful. Therefore, it is necessary to develop a fully 3D prognostic model for air pollution modeling in coastal areas.

Acknowledgments. This work has been supported by the project (No. 49135110) from the National Foundation of Natural Sciences.

REFERENCES

Caughey, S. J., and S. G. Palmer, 1979: Some aspects of turbulence structure through the depth of convective boundary layer. *Quart. J. Roy. Meteor. Soc.*, **105,** 811–827.

Deardorff, J. W., 1972: Numerical investigation of neutral and unstable planetary boundary layers. *J. Atmos. Sci.*, **29,** 91–115.

Donaldson, C. P., 1973: Construction of a dynamic model of the production of atmospheric turbulence and the dispersal of atmospheric pollutants. *Workshop on Micrometeorology,* D. A. Haugen, Ed., Amer. Meteor. Soc., 313–388.

Durand, P., S. Briere, and A. Druilhet, 1989: A sea–land transition observed during the COAST experiment. *J. Atmos. Sci.*, **46,** 96–116.

Fritts, T. W., F. J. Starheim, and B. J. Deihl, 1980: Formulation for defining the development of the TIBL in sea breeze flows. Preprints, *Second Conf. on Coastal Meteorology,* Los Angeles, CA, Amer. Meteor. Soc., 147–150.

Haugen, D. A., Ed., 1973: *Workshop on Micrometeorology.* Amer. Meteor. Soc., 397 pp.

Ludwig, F. L., 1985: A review of coastal zone meteorological processes important to the modeling of air pollution. *Air Pollution Modeling and Its Application,* Vol. IV, C. De. Wispelaere, Ed., Plenum Press, 225–258.

Mellor, G. L., and T. Yamada, 1974: A hierarchy of turbulence closure models for planetary boundary layers. *J. Atmos. Sci.*, **31,** 1791–1806.

Ministry of the Environment, 1980: The Nanticoke May/June 1979 field study. ARB-TDA Report No. 61–80, Ontario, Canada, 138 pp.

Ogawa, Y., T. Ohara, S. Wakamatsu, P. G. Diosey, and I. Uno, 1986: Observation of lake breeze penetration and subsequent development of the thermal internal boundary layer for the Nanticoke II shoreline diffusion experiment. *Bound.-Layer Meteor.*, **35,** 207–230.

Pielke, R. A., 1974: A three-dimensional numerical model of the sea breezes over South Florida. *Mon. Wea. Rev.*, **102,** 115–139.

——, 1984: *Mesoscale Meteorological Modeling.* Academic Press, 612 pp.

Reynolds, W. C., 1970: Computation of turbulent flows. State of the art. Dept. of Mechanical Engineering Report MD-27, Stanford University, Stanford, California.